nature physics

LETTERS

PUBLISHED ONLINE: 4 JANUARY 2016 | DOI: 10.1038/NPHYS3610

Strongly enhanced effects of Lorentz symmetry violation in entangled Yb^+ ions

V. A. Dzuba[1], V. V. Flambaum[1], M. S. Safronova[2,3]*, S. G. Porsev[2,4], T. Pruttivarasin[5], M. A. Hohensee[6] and H. Häffner[7]

A number of theories aiming at unifying gravity with other fundamental interactions, including field theory, suggest the violation of Lorentz symmetry[1–3]. Whereas the energy scale of such strongly Lorentz-symmetry-violating physics is much higher than that attainable at present by particle accelerators, Lorentz violation may nevertheless be detectable via precision measurements at low energies[2]. Here, we carry out a systematic theoretical investigation to identify which atom shows the greatest promise for detecting a Lorentz symmetry violation in the electron–photon sector. We found that the ytterbium ion (Yb^+) is an ideal system with high sensitivity, as well as excellent experimental controllability. By applying quantum-information-inspired technology to Yb^+, we expect tests of local Lorentz invariance (LLI) violating physics in the electron–photon sector to reach levels of 10^{-23}—five orders of magnitude more sensitive than the current best bounds[4–6].

It has been conjectured that Lorentz symmetry may be violated in string theories, with the Lorentz-violating effects being suppressed by some power of the ratio R between the electroweak scale and the natural (Planck) energy scale for strings: $R = m_{ew}/M_{pl} = 2 \times 10^{-17}$ (ref. 2). Therefore, the observable, but extremely small, Lorentz-violating effects may appear in low-energy experiments carried out with the corresponding high precision. Using the Yb^+ ion, as proposed in this work, will for the first time allow probing whether Lorentz violation is minimally suppressed at low energies for photons and electrons. If the Lorentz violation is not observed in the Yb^+ experiment proposed here, it will show that Lorentz violation in the photon–electron sector does not arise at this first-order level in strings, or cancellations are present between various Lorentz violation effects to nullify the combined result. With the proton and neutron tests already over the O(1) bound[7–9], such a result would demonstrate that if physics at the Planck scale violates Lorentz invariance, it is more than minimally suppressed at low energies for normal matter, setting restrictions on potential unification theories.

Separate violations of LLI are possible for each type of particle, making it essential to verify LLI in different systems at a high level of precision. As a result, LLI tests have been conducted for photons[5,10], protons[7], neutrons[8,9], electrons[4,6], muons[11] and neutrinos[12], with the detailed summary of all current limits given in ref. 1.

Testing LLI of the electron motion in a Coulomb potential created by a nucleus has the appeal of testing for new physics in a well-understood system. In these atomic experiments[4,6], one searches for variations of the atomic energy levels when the orientation of the electronic wavefunction is rotated with respect to the standard reference frame, such as the Sun-centred celestial-equatorial frame (SCCEF; ref. 13). The atomic experiments may be interpreted as Lorentz violation tests for the photon, electron, and nucleus constituents, such as the proton and neutron; with different experiments being sensitive to a different combination of LLI effects[14]. The most sensitive LLI tests for the electron have been conducted with neutral Dy atoms[4] and Ca^+ ions[6]. In this work, we explore the rest of the periodic table to answer the following question: which atomic system could most drastically improve tests of LLI in the electron–photon sector?

LLI-violating effects can be classified in the framework of the standard model extension (SME; refs 1,15,16). The SME is an effective field theory that maintains energy–momentum conservation, observer Lorentz covariance, and gauge invariance, but supplements the standard model Lagrangian with all combinations of the SM fields that are not term-by-term Lorentz invariant[15,16]. A particular advantage of the SME is the possibility to compare bounds on the Lorentz-violating parameters resulting from completely different experiments.

Here we focus on the term of the SME Lagrangian signifying the dependence of the maximally attainable velocity of a particle with respect to its propagation direction. We identify several factors that affect the precision of such a LLI test with atomic systems. First, it is crucial to use a state with a long lifetime to allow for a precise determination of the energy differences. Second, it is beneficial that the state has a strong sensitivity to LLI-violation effects in the electron–photon sector, that is, the size of the matrix element of the corresponding operator. The LLI-violating interaction[6] contains the second power of the momentum operator p. Therefore, the corresponding matrix elements are expected to be large for orbitals with large kinetic energy. This happens for the atomic $4f$-electrons localized deep inside the atom in the area of large potential and kinetic energy in some atomic systems. Last, we ask for a good theoretical understanding of the system and availability of already developed experimental techniques to carry out precision measurements.

We find that the metastable $4f^{13}6s^2\ ^2F_{7/2}$ state of Yb^+ has extremely favourable characteristics, such as being very sensitive to LLI violations as well has having an exceptionally long lifetime—of the order of ten years (ref. 17). In addition, the experimental methods for Yb^+ are well developed in the context of atomic clocks and the search for variation of fundamental constants. In particular, the electric-octupole E3 transition between the $4f^{13}6s^2\ ^2F_{7/2}$ excited state

[1]School of Physics, University of New South Wales, Sydney 2052, Australia. [2]Department of Physics and Astronomy, University of Delaware, Newark, Delaware 19716, USA. [3]Joint Quantum Institute, National Institute of Standards and Technology and the University of Maryland, College Park, Maryland 20742, USA. [4]Petersburg Nuclear Physics Institute, Gatchina, Leningrad District 188300, Russia. [5]Quantum Metrology Laboratory, RIKEN, Wako, Saitama 351-0198, Japan. [6]Lawrence Livermore National Laboratory, Livermore, California 94550, USA. [7]Department of Physics, University of California, Berkeley, California 94720, USA. *e-mail: msafrono@udel.edu

and the ground state[18–20] has been studied in detail for these applications. Yb^+ ions are also used in quantum information research[21]. As a result, the Yb^+ ion is a well-studied system for precision control and manipulation of its atomic states, making it particularly well-suited to searches for the Lorentz violation signature.

The effect of various sources of Lorentz violation on atomic frequencies has been discussed in ref. 14. Here, we follow the formalism of ref. 6, in which a possible Lorentz violation in light manifests itself in the electronic SME Lagrangian, which is given by (in atomic units)

$$\mathcal{L}=\frac{1}{2}i\bar{\psi}(\gamma_\nu+c'_{\mu\nu}\gamma^\mu)\overleftrightarrow{D}^\nu\psi-\bar{\psi}\psi \qquad (1)$$

where ψ is a Dirac spinor, γ^μ are the Dirac matrices, $\bar{\psi}\overleftrightarrow{D}^\nu\psi\equiv\bar{\psi}D^\nu\psi-\psi D^\nu\bar{\psi}$, with D^ν being the covariant derivative. The tensor $c'_{\mu\nu}=c_{\mu\nu}+k_{\mu\nu}/2$ that characterizes the LLI-violation effects contains Lorentz-violation parameters from both the electron ($c_{\mu\nu}$) and the photon ($k_{\mu\nu}$) sectors[1,2].

Experiments with $^{173}Yb^+$ ions are also sensitive to violations of LLI for the neutron and the proton[14,22]. Moreover, the nucleus of $^{173}Yb^+$ is deformed and has an order-of-magnitude enhanced electric quadrupole moment and time-reversal violating magnetic quadrupole moment as compared to a spherical nucleus[23,24]. A similar enhancement may exist for the nuclear LLI violation determined by the tensor $\langle p^2\rangle-3\langle p_z^2\rangle$. Because we expect to surpass the energy resolution of 5 mHz for the proton test[7] considerably, an experimental signature of LLI violation in a $^{173}Yb^+$ experiment could come either from the electron–photon or the nuclear sector. The even Yb nuclei, which have zero nuclear spin and quadrupole moment, are not sensitive to violation of LLI of either protons or the neutron. Because the Yb^+ LLI test involves monitoring quadrupole energy shifts, nuclear LLI effects will not contribute for the spin-1/2 nucleus $^{171}Yb^+$, where nuclear LLI could produce only dipole energy shifts. Therefore, the electron/photon and nuclear sectors can be disentangled by comparing the LLI-violation signal from $^{173}Yb^+$ with that of the other isotopes, resulting in clean LLI bounds.

From equation (1), violations of Lorentz invariance and Einstein's equivalence principle in bound electronic states result in a small shift of the energy levels described by a Hamiltonian[4,14]

$$\delta H=-\left(C_0^{(0)}-\frac{2U}{3c^2}c_{00}\right)\frac{\mathbf{p}^2}{2}-\frac{1}{6}C_0^{(2)}T_0^{(2)} \qquad (2)$$

where $\mathbf{p}$ is the momentum of a bound electron, c is the speed of light, and U is the Newtonian gravitational potential. The parameters $C_0^{(0)}$, c_{00} and $C_0^{(2)}$ contain elements of the $c'_{\mu\nu}$ tensor[6]. The relativistic form of the $\mathbf{p}^2$ operator is $c\gamma_0\gamma^j p_j$. The non-relativistic form of the $T_0^{(2)}$ operator is $T_0^{(2)}=\mathbf{p}^2-3p_z^2$, and the relativistic form is $T_0^{(2)}=c\gamma_0\left(\gamma^j p_j-3\gamma^3 p_3\right)$, with z (the third spatial component) defined by the quantization axis.

The $c'_{\mu\nu}$ tensor is frame-dependent, but its value may be uniquely specified in the SCCEF (ref. 13). Because of the Earth's motion, time-dependent Lorentz transformations from the SCCEF to the local laboratory frame give rise to time-dependence of the local observables that involve any of the $C_0^{(0)}$, c_{00} and/or $C_0^{(2)}$ parameters. The elements c_{JK} in $c'_{\mu\nu}$, where $J,K=\{1,2,3\}$ (spatial components), which describe the dependence of the kinetic energy on the direction of the momentum, have a leading-order time-modulation period related to the sidereal day (12-h and 24-h modulation). Other elements, c_{TJ} (where $T=0$) and c_{00}, describe the dependence of the kinetic energy on the boost of the laboratory frame, and have a leading-order time-modulation period related to the sidereal year.

The Yb^+ ground state has the configuration $[Xe]4f^{14}6s$, and is essentially a heavier analogue of Ca^+, which was used in the most recent experiment[6], but has an additional set of states resulting from excitation of the filled $4f$ shell. Yb^+ also has a metastable excited $5d_{5/2}$ state analogue to Ca^+. However, the $4f$ shell in Yb^+ is localized much deeper in the atom than the $6s$ or any other valence states, such as the $5d$ state. As a result, we expect the $4f^{13}6s^2\,{}^2F_{7/2}$ metastable level of Yb^+ to be very sensitive to Lorentz-violating effects. Indeed, we find that the LLI-sensitive $T_0^{(2)}$ matrix element for this state is over an order of magnitude larger than for the $4f^{14}5d$ states (Methods). The results of the calculations are summarized in Table 1, where we also list reduced $T^{(2)}$ matrix elements defined in Methods for the nd states of Ca^+, Ba^+ and Yb^+, which all have similar values.

Table 1 | Reduced matrix elements of the $T^{(2)}$ operator in Ca^+, Ba^+, Yb^+ ions in atomic units.

Ion	State	$\langle J\|\|T^{(2)}\|\|J\rangle$
Ca^+	$3d\,{}^2D_{3/2}$	7.09(12)
	$3d\,{}^2D_{5/2}$	9.25(15)
Ba^+	$5d\,{}^2D_{3/2}$	6.83
	$5d\,{}^2D_{5/2}$	8.65
Yb^+	$4f^{14}5d\,{}^2D_{3/2}$	9.96
	$4f^{14}5d\,{}^2D_{5/2}$	12.08
	$4f^{13}6s^2\,{}^2F_{7/2}$	−135.2

Ca^+ values are from ref. 6.

In a non-zero magnetic field, the excited state $4f^{13}6s^2\,{}^2F_{7/2}$ of Yb^+ will split into eight substates, with magnetic quantum numbers $m_f=\pm1/2,\ \pm3/2,\ \pm5/2,\ \pm7/2$ for even isotopes with no hyperfine structure. These four pairs of states will experience different energy shifts in the case of a detectable Lorentz-violation signal (see Fig. 1). The maximum Lorentz-violation signal will then be observed by monitoring the frequency difference between $m_f=|1/2|$ and $m_f=|7/2|$ states expressed in terms of the Lorentz-violating parameter $C_0^{(2)}$ as

$$\frac{1}{h}\left(E_{m_f=7/2}-E_{m_f=1/2}\right)=6.14\times10^{16}\,\mathrm{Hz}\cdot C_0^{(2)} \qquad (3)$$

This gives an enhancement by a factor of 14 in comparison to Ca^+ (ref. 6) owing to the increased $T^{(2)}$ matrix element.

The odd ^{171}Yb isotope has nuclear spin $I=1/2$, leading to a splitting of the $4f^{13}6s^2\,{}^2F_{7/2}$ level into two levels with total angular momenta $F=3$ and $F=4$ (Fig. 2). In a magnetic field, $F=3$ level will split into seven sub-levels ($m_F=-3\ldots3$) and $F=4$ level will split into nine sub-levels ($m_F=-4\ldots4$). The ^{173}Yb isotope has nuclear spin $I=5/2$, leading to more complicated level structure. For odd isotopes, the energy difference between magnetic hyperfine m_F substates will be monitored.

Below, we discuss a procedure to detect potential LLI violations by measuring the energy difference between the $m_f=|7/2|$ and $m_f=|1/2|$ states in the $4f^{13}6s^2\,{}^2F_{7/2}$ manifold in Yb^+.

Typically, the main source of noise in such measurements is due to magnetic field fluctuations. To remove this noise, the work of ref. 6 used a superposition of two ions with a state prepared in a decoherence-free subspace (DFS; ref. 25). To implement the DFS technique with two trapped Yb^+ ions, one will monitor the phase evolution difference of the state $|\Psi\rangle=(1/\sqrt{2})(|1/2,-1/2\rangle+|7/2,-7/2\rangle)$, where $|m_1,m_2\rangle$ represents the state with $m_f=m_1$ and m_2 for the first and second ion, respectively, in the $F_{7/2}$ manifold. The target state $|\Psi\rangle$ can be prepared by creating a product state, $|\Psi'\rangle=(1/2)\,(|-1/2\rangle+|-7/2\rangle)\otimes(|+1/2\rangle+|+7/2\rangle)$, which dephases into a mixed state that contains $|\Psi\rangle$ with 50% probability. With additional experimental complications, a direct preparation of an entangled state would result in an increase of the signal-to-noise ratio by a factor of two.

Starting from the ground state of Yb^+, the state $|\Psi\rangle=(1/\sqrt{2})(|1/2,-1/2\rangle+|7/2,-7/2\rangle)$ can be prepared with

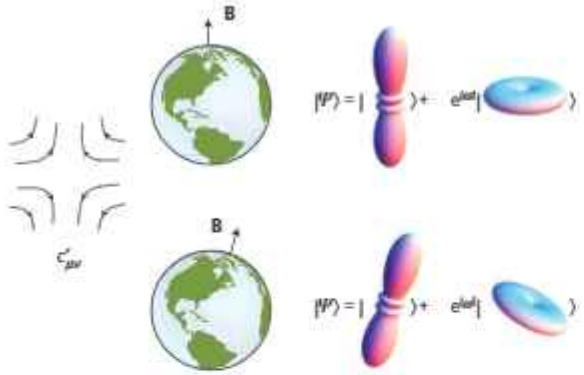

Figure 1 | The Lorentz-violating signal will manifest itself as the change of the energy difference between $m_J = |1/2|$ and $m_J = |7/2|$ states. The orthogonal orientations of the electronic wavefunction of the $4f^{13}6s^2\,{}^2F_{7/2}$ m_J manifold in Yb^+, with $m_J = |1/2|$ and $m_J = |7/2|$, will have a different response to the Lorentz-violating effect quantified by the $c'_{\mu\nu}$ tensor. This results in a modulation of the energy difference between these two states as the Earth rotates the wavefunction with respect to the Sun-centred celestial-equatorial frame. The total electronic wavefunction is in superposition of the two states. The orientation of the wavefunction will be given by the direction of the magnetic field **B**, assumed to be fixed in the laboratory frame.

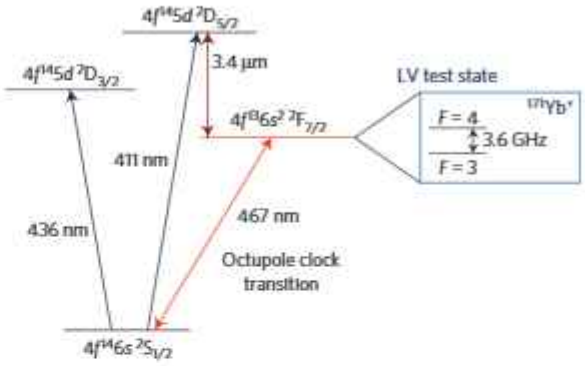

Figure 2 | Relevant energy levels of Yb^+. The hyperfine splitting is shown for the $4f^{13}6s^2\,{}^2F_{7/2}$ state of the $^{171}Yb^+$ isotope.

$\pi/2$ and π pulses using the coherent control developed for the implementation of the octupole $^2S_{1/2}$–$^2F_{7/2}$ atomic clock[18,19]. Alternatively, one can also implement $\pi/2$ and π pulses by driving Raman transitions by means of the $^2D_{5/2}$ state with 411 nm and 3.4 μm laser light (Fig. 2). For the odd $^{171}Yb^+$ (inset in Fig. 2) and $^{173}Yb^+$ isotope, one can prepare the target state with radiofrequency pulses, after populating a pure state in the $^2F_{7/2}$ manifold.

Another factor that will greatly improve the limits of the Lorentz-violating parameters obtained from measurements with Yb^+ is the long lifetime of its excited state. In particular, because the lifetime of the $^2F_{7/2}$ state of Yb^+ is in the range of several years (ref. 20), the Ramsey duration of the proposed experiment with Yb^+ is not limited by spontaneous decay. Instead, the coherence of the target state in the DFS is likely to be limited by the stability of the magnetic field gradient in the vicinity of the ions. It has been shown that in a magnetically unshielded environment, ions can retain entanglement in the DFS for up to 30 s (ref. 26). Hence, in a magnetically shielded trap, we can expect to suppress decoherence due to magnetic field noise such that Ramsey durations for much longer times are realistic.

An additional complication with long Ramsey interrogation times is that motional heating of the ion degrades the fidelity of the analysis pulses. For instance, the experiment in ref. 6 with $^{40}Ca^+$ was performed with a Ramsey duration of 100 ms because of this motional heating. This problem can be either addressed with sympathetic cooling just before state read-out using auxiliary Yb ions, similar to preliminary work demonstrating this with $^{40}Ca^+$ (ref. 27), or by employing ion traps providing sufficiently low motional heating rates, such as the ones typically used in quantum information processing experiments[26].

We estimate that, with a Ramsey time of 60 s and two fully entangled Yb^+ ions, the parameter $C_9^{(2)}$ will be bounded at the level of $8.5 \times 10^{-20}/\sqrt{\tau/\mathrm{sec}}$, where τ is the measurement time (Methods)—an improvement of ~4,800 times over the measurement with $^{40}Ca^+$ (ref. 6). At this level of sensitivity, we expect that the c_{jk} parameters will be bounded at the level of 3×10^{-22} and 1.5×10^{-23} for a day-long and year-long measurement, respectively. The c_{tj} terms, which are sensitive to the velocity of the laboratory frame, are suppressed by a factor of 10^{-4} owing to the relatively small Earth's velocity in the SCCEF as compared to the speed of light. With a year-long measurement, one expects to be sensitive to the c_{tj} parameters at the level of 1.5×10^{-19}, a factor of 6,000 improvement over the current best limits[4].

Systematics which can directly affect the energy of our target states are magnetic and electric field fluctuations in the vicinity of the ions. Both fields can be measured directly using the ions themselves as a probe. We can then correct for the effects of the differential linear Zeeman shift between the two ions due to a finite magnetic field gradient across the ion string, the quadratic Zeeman shift, and the Stark shift from the oscillating electric field from the trap. A change in the environmental temperature during the measurement can also affect the energy shift through the black-body radiation (BBR). The BBR shift between the two Zeeman states ($m_J = 1/2$ and $m_J = 7/2$) of the $F_{7/2}$ manifold depends on the anisotropy of the BBR source. By assuming that the temporal temperature variation of the environment is less than 0.1 K, we estimate that, in the worst case scenario of a maximal anisotropy of 100%, the differential BBR shift between the two Zeeman states is ~1 μHz (ref. 28), which affects the sensitivity of c_{jk} at the 6×10^{-24} level. Finally, we estimate that the systematic error due to the AC-Stark effect of laser interaction is negligible for the proposed experiment (Methods).

Our calculations also identified general rules for the enhancement of the reduced matrix elements of the $T^{(2)}$ operator. We find that the only parameter that significantly affects the matrix elements leading to the tensor Lorentz violation sensitivity is the deeper localization of the probe electron where the kinetic energy $\mathbf{p}^2/2$ and $T^{(2)} \propto \mathbf{p}^2$ are larger. We find that an expectation value $\langle\psi|r|\psi\rangle < 0.8$ a.u. of the corresponding electron is a good indicator of the large value of the $T^{(2)}$ matrix element. This condition is satisfied for the $4f$ hole states, such as the Yb^+ state considered here, or for highly charged ions with nf valence electrons and charges of ~15 (ref. 29). Such systems with configurations containing two $4f$ electrons or two $4f$ holes can have an extra enhancement by a factor of two, and a higher degree of ionization leads to a further increase in the $T^{(2)}$ matrix element values. Other lanthanide ions, for example the Tm^+ ion with $4f^{13}6s$ ground state, may provide other potential candidates for Lorentz violation tests. We also considered the Th^{3+} ion owing to its $5f_{5/2}$ ground state. Laser cooling was demonstrated for this ion in ref. 30, but we find that the corresponding $T^{(2)}$ matrix element is more than a factor of three smaller than the one in Yb^+. The $5f$ orbital here is a valence orbital rather than a hole in the filled shell; moreover the $4f$ electron is generally deeper localized than the $5f$ electron.

Owing to the increased sensitivity to LLI violation and long lifetime of the metastable $F_{7/2}$ state of Yb^+, we estimate that experiments can reach the sensitivities of 1.5×10^{-23} for the c_{jk} parameters, improving the current best limits[6] by more than a factor of 10^5. Moreover, the projected sensitivity of the c_{tj} parameters will be at the level of 1.5×10^{-19}. In the electron–photon sector, this

would for the first time probe all tensor Lorentz-violating elements below the ratio between the electroweak and Planck energy scales[2].

Methods

Methods and any associated references are available in the online version of the paper.

Received 21 July 2015; accepted 19 November 2015; published online 4 January 2016

References

1. Kostelecký, V. A. & Russell, N. Data tables for Lorentz and CPT violation. *Rev. Mod. Phys.* **83,** 11–32 (2011).
2. Kostelecký, V. A. & Potting, R. CPT, strings, and meson factories. *Phys. Rev. D* **51,** 3923–3935 (1995).
3. Pospelov, M. & Shang, Y. Lorentz violation in Horava–Lifshitz-type theories. *Phys. Rev. D* **85,** 105001 (2012).
4. Hohensee, M. A. *et al.* Limits on violations of Lorentz symmetry and the Einstein equivalence principle using radio-frequency spectroscopy of atomic dysprosium. *Phys. Rev. Lett.* **111,** 050401 (2013).
5. Nagel, M. *et al.* Direct terrestrial test of Lorentz symmetry in electrodynamics to 10^{-18}. *Nature Commun.* **6,** 8174 (2015).
6. Pruttivarasin, T. *et al.* Michelson–Morley analogue for electrons using trapped ions to test Lorentz symmetry. *Nature* **517,** 592–595 (2015).
7. Wolf, P., Chapelet, F., Bize, S. & Clairon, A. Cold atom clock test of Lorentz invariance in the matter sector. *Phys. Rev. Lett.* **96,** 060801 (2006).
8. Allmendinger, F. *et al.* New limit on Lorentz-Invariance- and CPT-violating Neutron Spin interactions using a free-spin-precession ^{3}He-^{129}Xe comagnetometer. *Phys. Rev. Lett.* **112,** 110801 (2014).
9. Smiciklas, M., Brown, J. M., Cheuk, L. W., Smullin, S. J. & Romalis, M. V. New test of local Lorentz invariance using a ^{21}Ne–Rb–K comagnetometer. *Phys. Rev. Lett.* **107,** 171604 (2011).
10. Eisele, Ch, Nevsky, A. Yu & Schiller, S. Laboratory test of the isotropy of light propagation at the 10^{-17} level. *Phys. Rev. Lett.* **103,** 090401 (2009).
11. Bennett, G. W. *et al.* Muon $g-2$ Collaboration. Search for Lorentz and CPT violation effects in muon spin precession. *Phys. Rev. Lett.* **100,** 091602 (2008).
12. Adamson, P. *et al.* (The MINOS Collaboration) Search for Lorentz invariance and *CPT* violation with muon antineutrinos in the MINOS Near Detector. *Phys. Rev. D* **85,** 031101 (2012).
13. Kostelecký, V. A. & Mewes, M. Signals for Lorentz violation in electrodynamics. *Phys. Rev. D* **66,** 056005 (2002).
14. Kostelecký, V. A. & Lane, C. D. Constraints on Lorentz violation from clock-comparison experiments. *Phys. Rev. D* **60,** 116010 (1999).
15. Colladay, D. & Kostelecký, V. A. CPT violation and the standard model. *Phys. Rev. D* **55,** 6760–6774 (1997).
16. Colladay, D. & Kostelecký, V. A. Lorentz-violating extension of the standard model. *Phys. Rev. D* **58,** 116002 (1998).
17. Roberts, M. *et al.* Observation of an electric Octupole transition in a single ion. *Phys. Rev. Lett.* **78,** 1876–1879 (1997).
18. Huntemann, N. *et al.* Improved limit on a temporal variation of m_p/m_e from comparisons of Yb^+ and Cs atomic clocks. *Phys. Rev. Lett.* **113,** 210802 (2014).
19. Godun, R. M. *et al.* Frequency ratio of two optical clock transitions in $^{171}Yb^+$ and constraints on the time variation of fundamental constants. *Phys. Rev. Lett.* **113,** 210801 (2014).
20. Huntemann, N. *et al.* High-accuracy optical clock based on the octupole transition in $^{171}Yb^+$. *Phys. Rev. Lett.* **108,** 090801 (2012).
21. Islam, R. *et al.* Emergence and frustration of magnetism with variable-range interactions in a quantum simulator. *Science* **340,** 583–587 (2013).
22. Stadnik, Y. V. & Flambaum, V. V. Nuclear spin-dependent interactions: searches for WIMP, axion and topological defect dark matter, and tests of fundamental symmetries. *Eur. Phys. J. C* **75,** 110 (2015).
23. Flambaum, V. V. Spin hedgehog and collective magnetic quadrupole moments induced by parity and time invariance violating interaction. *Phys. Lett. B* **320,** 211–215 (1994).
24. Flambaum, V. V., DeMille, D. & Kozlov, M. G. Time-reversal symmetry violation in molecules induced by nuclear magnetic quadrupole moments. *Phys. Rev. Lett.* **113,** 103003 (2014).
25. Roos, C. F., Chwalla, M., Kim, K., Riebe, M. & Blatt, R. 'Designer atoms' for quantum metrology. *Nature* **443,** 316–319 (2006).
26. Häffner, H. *et al.* Robust entanglement. *Appl. Phys. B* **81,** 151–153 (2005).
27. Pruttivarasin, T. *Spectroscopy, Fundamental Symmetry Tests and Quantum Simulation with Trapped Ions* PhD thesis, Univ. California (2014).
28. Flambaum, V. V., Porsev, S. G. & Safronova, M. S. Energy shift due to anisotropic black body radiation. Preprint at http://arXiv.org/abs/1508.01242 (2015).
29. Safronova, M. S. *et al.* Highly-charged ions for atomic clocks, quantum information, and search for α-variation. *Phys. Rev. Lett.* **113,** 030801 (2014).
30. Campbell, C. J. *et al.* Multiply charged thorium crystals for nuclear laser spectroscopy. *Phys. Rev. Lett.* **102,** 233004 (2009).

Acknowledgements

M.S.S. thanks the School of Physics at UNSW, Sydney, Australia for hospitality and acknowledges support from the Gordon Godfrey Fellowship programme, UNSW. This work was supported by the NSF CAREER Program grant # PHY 0955650, NSF grants # PHY 1212442, # PHY 1404156, # PHY 1507160 and # PHY 1520993, the Australian Research Council and was performed under the auspices of the US Department of Energy by Lawrence Livermore National Laboratory under Contract DE-AC52-07NA27344. T.P. is supported by RIKEN's Foreign Postdoc Researcher Program.

Author contributions

V.A.D. had the idea to use Yb^+ and identified the enhancement to the Lorentz violation violation. V.A.D., V.V.F., M.S.S. and S.G.P. carried out atomic calculations. T.P., M.A.H. and H.H. worked out the experimental scheme considerations and projected the Lorentz violation limits. All authors contributed to the discussions of the results and manuscript.

Additional information

Reprints and permissions information is available online at www.nature.com/reprints. Correspondence and requests for materials should be addressed to M.S.S.

Competing financial interests

The authors declare no competing financial interests.

Methods

Calculation of the matrix elements. The calculations of the energy shift due to LLI violation reduce to a calculation of the expectation value of the Hamiltonian in equation (2). The matrix element of $\langle Jm_J|\mathbf{p}^2-3p_z^2|Jm_J\rangle$ is expressed through the reduced matrix element of the $T^{(2)}$ operator using the Wigner–Eckart theorem

$$\langle Jm_J|T^{(2)}_0|Jm_J\rangle=(-1)^{J-m_J}\begin{pmatrix} J & 2 & J \\ -m_J & 0 & m_J\end{pmatrix}\langle J||T^{(2)}||J\rangle$$

Using the algebraic expression for the 3*j*-symbol, we arrive at the following expression for the matrix element of the $\langle Jm_J|\mathbf{p}^2-3p_z^2|Jm_J\rangle$ operator:

$$\langle Jm_J|T^{(2)}_0|Jm_J\rangle=\frac{-J(J+1)+3m_J^2}{\sqrt{(2J+3)(J+1)(2J+1)J(2J-1)}}\times\langle J||T^{(2)}||J\rangle$$

The angular factors are different for the Yb^+ $4f^{13}6s^2\ ^2F_{7/2}$ state and the Ca^+ $3d\ ^2D_{5/2}$ state, resulting in total enhancement of the Yb^+ LLI energy shift (equation (3)) of 13.8 in comparison with Ca^+ case, whereas reduced matrix elements $\langle J||T^{(2)}||J\rangle$ differ by a factor of 14.6.

The all-order method gave very accurate values of the $3d_J$ lifetimes[31] and quadrupole moments[32] in Ca^+. In the all-order method, single, double, and partial triple excitations of Dirac–Hartree–Fock wavefunctions are included to all orders of perturbation theory. We refer the reader to review ref. 33 for the description of the all-order method and its applications. The Ca^+ all-order results are accurate to about 1.5% (ref. 6). The calculations were carried out with both non-relativistic and relativistic operators; the differences were found to be negligible at the present level of accuracy. The results are listed in Table 2.

The all-order method was designed to work for monovalent systems and is not applicable to the calculation of $4f^{13}6s^2\ ^2F_{7/2}$ properties owing to the electronic configuration of this state, which has a hole in the $4f$ shell. We used both a one-electron Dirac–Fock calculation and a large-scale configuration interaction calculation for this state and find excellent agreement of both approaches. The 15-electron configuration interaction calculation follows the approach described in ref. 34. Briefly, we start from the solution of the Dirac–Fock equations and carry out the initial self-consistency procedure for the $[1s^2,\ldots,4f^{14},6p]$ configuration. The $6s$ orbital was constructed for the $4f^{13}6s^2$ configuration, and the $5d_{3/2,5/2}$ orbitals were constructed for the $4f^{13}5d6s$ configuration. The basis set used in the CI calculations included virtual orbitals up to $8s$, $8p$, $7d$, $7f$ and $5g$. The virtual orbitals were constructed as described in refs 35,36. The configuration space was formed by allowing single and double excitations for the odd-parity states from the $4f^{14}6p$, $4f^{13}6s^2$ and $4f^{13}5d6s$ configurations to virtual orbitals of the basis set listed above.

We have verified the convergence of the CI by carrying out three calculations with an increasing set of configuration functions: including single and double (SD) excitations to the $6s$, $6p$, $5d$ and $5f$ orbitals (we designate it $[6sp5df]$); adding excitations to the $7s$, $7p$, $6d$, $6f$ and $5g$ orbitals $[7sp6df5g]$; and also adding $8s$, $8p$, $7d$ and $7f$ orbitals $[8sp7df5g]$. The last configuration set results in rather lengthy calculations with ~2,300,000 determinants.

As demonstrated in Table 2, the number of included configurations has only a negligible effect on the $T^{(2)}$ operator of the $4f^{13}6s^2\ ^2F_{7/2}$ state. The result of the configuration interaction calculation is in agreement with a simple DF calculation. Inclusion of the random-phase approximation changes this value by 6%.

Estimation of the sensitivity of the experiment. The sensitivity of the frequency variation can be estimated from the quantum projection noise of the measurement:

$$\sigma_f=\frac{1}{4\pi A\sqrt{T}}\cdot\frac{1}{\sqrt{\tau}}$$

where A is the amplitude of the Ramsey oscillation signal, T is the Ramsey duration and τ is the measurement time. Assuming that the target state $|\Psi\rangle=(1/\sqrt{2})(|1/2,-1/2\rangle+|7/2,-7/2\rangle)$ for $^2F_{7/2}$ is prepared through the creation of a mixed state, as demonstrated in ref. 6, then the amplitude of the Ramsey oscillation is $A=0.5$. With a Ramsey duration of 60 s, the estimated sensitivity is $\sim 0.02/\sqrt{\tau/\mathrm{Hz}}$. Together with the improved sensitivity of the atomic state to Lorentz violation, as given in equation (3), we estimate that the parameter $C_0^{(2)}$ will be bounded at the level of $1.7\times10^{-19}/\sqrt{\tau/\mathrm{sec}}$ for two ions, which is an improvement of ~2,400 times over the measurement with $^{40}Ca^+$ (ref. 6). Use of the pure entangled two-ion states ($A=1$) would improve these bounds by an additional factor of two, resulting in a sensitivity of the $C_0^{(2)}$ at the level of $8.5\times10^{-20}/\sqrt{\tau/\mathrm{sec}}$—an improvement of ~4,800 times over the measurement with $^{40}Ca^+$ (ref. 6).

Table 2 | Reduced matrix elements of the $T^{(2)}$ operator in Yb^+ ion in atomic units.

State	Method	$\langle J\|\|T^{(2)}\|\|J\rangle$
$4f^{14}5d\ ^2D_{3/2}$	LCCSD	9.96
$4f^{14}5d\ ^2D_{5/2}$	DF	7.23
	CI $7sp6df5g$	11.6
	LCCSD	12.08
$4f^{13}6s^2\ ^2F_{7/2}$	DF	−145
	CI $6sp5df$	−143.8
	CI+RPA $6sp5df$	−135.1
	CI+RPA $7sp6df5g$	−135.6
	CI+RPA $8sp6df5g$	−135.2

Method of calculations is listed in the column 'Method'. LCCSD is the linearized coupled-cluster method with single and double excitations, DF is the Dirac–Fock method, RPA is the random-phase approximation, and CI is the configuration interaction. We list the included configurations for the 15-electron CI calculation.

Systematic effects due to the AC-Stark effect. We now discuss the impact of the substantial AC-Stark shift when driving the weak octupole transition from the ground state to the $^2F_{7/2}$ state. For instance, in the experiments in ref. 20, for each π pulse an AC-Stark-effect-related phase of the order of $2\pi\times3.3$ rad was accumulated. However, for the odd Yb-isotopes the desired superposition state can be achieved by driving microwave transitions between hyperfine levels of the $F_{7/2}$ manifold. Hence, driving the octupole transition (or alternatively the Raman transition via the D-states) is only required to populate a single Zeeman state of the $F_{7/2}$ manifold as well as to probe for its population after the Ramsey sequence. Thus, the AC-Stark effect associated with driving the octupole transition has no impact on the actual phase evolution.

For the even isotopes it is possible to find state preparation schemes where the AC-Stark shift cancels between both ions, to the degree the ions are illuminated by the same amount. In such a scheme, the two ions would be prepared in the two distinct Zeeman states of the ground state, $m_J=\pm1/2$. A common two-frequency laser field would prepare the desired superposition state on the different Zeeman transitions via the $\pi/2$ pulse driving the $m_J=1/2\rightarrow m_J=7/2$ transition on the first ion and the $m_J=-1/2\rightarrow m_J=-1/2$ transition on the second ion. The preparation concludes with a π pulse on the $m_J=1/2\rightarrow m_J=1/2$ transition on the first ion and the $m_J=-1/2\rightarrow m_J=-7/2$ transition on the second ion. This sequence leads to an equal phase due to the AC-Stark effect of the relevant $|1/2,-1/2\rangle$ and $|7/2,-7/2\rangle$ states, and hence the AC-Stark effect drops out. We estimate that using an intensity stability of 10^{-2} and illuminating both ions to within 10^{-3} equally will suppress the residual Stark-shift-related phase to $2\pi\times2\times10^{-4}$ rad, well below the quantum projection noise of 100 experimental cycles of $2\pi\times1.6\times10^{-2}$ rad, after which the intensities could be re-calibrated.

We conclude by stating that the expected AC-Stark effect when preparing the $F_{7/2}$ with Raman transitions via the D-states requires less power than via the octupole transition, so the AC-Stark effect should pose no hurdle for this route either.

References

31. Kreuter, A. *et al.* Experimental and theoretical study of the $3d^2D$–level lifetimes of $^{40}Ca^+$. *Phys. Rev. A* **71,** 032504 (2005).
32. Jiang, D., Arora, B. & Safronova, M. S. Electric quadrupole moments of metastable states of Ca^+, Sr^+, and Ba^+. *Phys. Rev. A* **78,** 022514 (2008).
33. Safronova, M. S. & Johnson, W. R. All-order methods for relativistic atomic structure calculations. *Adv. At. Mol. Opt. Phys.* **55,** 050401 (2008).
34. Porsev, S. G., Safronova, M. S. & Kozlov, M. G. Correlation effects in Yb^+ and implications for parity violation. *Phys. Rev. A* **86,** 022504 (2012).
35. Bogdanovich, P. Usage of transformed functions for calculations of electric dipole transitions. *Lith. Phys. J.* **31,** 79–83 (1991).
36. Kozlov, M. G., Porsev, S. G. & Flambaum, V. V. Manifestation of the nuclear anapole moment in the M1 transitions in bismuth. *J. Phys. B* **29,** 689–697 (1996).